

CAPERS Observations of Two UV-Bright Galaxies at $z > 10$. More Evidence for Bursting Star Formation in the Early Universe.

VASILY KOKOREV,¹ ÓSCAR A. CHÁVEZ ORTIZ,¹ ANTHONY J. TAYLOR,¹ STEVEN L. FINKELSTEIN,¹
PABLO ARRABAL HARO,^{2,*} MARK DICKINSON,³ JOHN CHISHOLM,¹ SELJI FUJIMOTO,¹ JULIAN B. MUÑOZ,¹ RYAN ENDSLEY,¹
WEIDA HU,^{4,5} LORENZO NAPOLITANO,^{6,7} STEPHEN M. WILKINS,^{8,9} HOLLIS B. AKINS,¹ RICARDO AMORIÍN,¹⁰
CAITLIN M. CASEY,^{11,12} YINGJIE CHENG,¹³ NIKKO J. CLERI,^{14,15,16} JUSTIN COLE,^{4,5} FERGUS CULLEN,¹⁷
EMANUELE DADDI,¹⁸ KELCEY DAVIS,¹⁹ CALLUM T. DONNAN,³ JAMES S. DUNLOP,¹⁷ VITAL FERNÁNDEZ,²⁰
MAURO GIAVALISCO,¹³ NORMAN A. GROGIN,²¹ NIMISH HATHI,²¹ MICHAELA HIRSCHMANN,²² JEYHAN S. KARTALTEPE,²³
ANTON M. KOEKEMOER,²¹ HO-HIN LEUNG,¹⁷ RAY A. LUCAS,²¹ DEREK MCLEOD,¹⁷ CASEY PAPOVICH,^{24,25}
LAURA PENTERICCI,⁶ PABLO G. PÉREZ-GONZÁLEZ,²⁶ RACHEL S. SOMERVILLE,²⁷ XIN WANG,^{28,29,30} L. Y. AARON YUNG,²¹
AND JORGE A. ZAVALA¹³

¹*Department of Astronomy, The University of Texas at Austin, Austin, TX 78712, USA*

²*Astrophysics Science Division, NASA Goddard Space Flight Center, 8800 Greenbelt Rd, Greenbelt, MD 20771, USA*

³*NSF's National Optical-Infrared Astronomy Research Laboratory, 950 N. Cherry Ave., Tucson, AZ 85719, USA*

⁴*Department of Physics and Astronomy, Texas A&M University, College Station, TX 77843-4242, USA*

⁵*George P. and Cynthia Woods Mitchell Institute for Fundamental Physics and Astronomy, Texas A&M University, College Station, TX 77843-4242, USA*

⁶*INAF – Osservatorio Astronomico di Roma, via Frascati 33, 00078, Monteporzio Catone, Italy*

⁷*Dipartimento di Fisica, Università di Roma Sapienza, Città Universitaria di Roma - Sapienza, Piazzale Aldo Moro, 2, 00185, Roma, Italy*

⁸*Astronomy Centre, University of Sussex, Falmer, Brighton BN1 9QH, UK*

⁹*Institute of Space Sciences and Astronomy, University of Malta, Msida MSD 2080, Malta*

¹⁰*Instituto de Astrofísica de Andalucía (CSIC), Apartado 3004, 18080 Granada, Spain*

¹¹*Department of Physics, University of California, Santa Barbara, CA 93106, USA*

¹²*Cosmic Dawn Center (DAWN), Niels Bohr Institute, University of Copenhagen, Jagtvej 128, København N, DK-2200, Denmark*

¹³*University of Massachusetts Amherst, 710 North Pleasant Street, Amherst, MA 01003-9305, USA*

¹⁴*Department of Astronomy and Astrophysics, The Pennsylvania State University, University Park, PA 16802, USA*

¹⁵*Institute for Computational and Data Sciences, The Pennsylvania State University, University Park, PA 16802, USA*

¹⁶*Institute for Gravitation and the Cosmos, The Pennsylvania State University, University Park, PA 16802, USA*

¹⁷*Institute for Astronomy, University of Edinburgh, Royal Observatory, Edinburgh EH9 3HJ, UK*

¹⁸*Université Paris-Saclay, Université Paris Cité, CEA, CNRS, AIM, 91191 Gif-sur-Yvette, France*

¹⁹*Department of Physics, 196A Auditorium Road, Unit 3046, University of Connecticut, Storrs, CT 06269, USA*

²⁰*Michigan Institute for Data Science, University of Michigan, 500 Church Street, Ann Arbor, MI 48109, USA*

²¹*Space Telescope Science Institute, 3700 San Martin Drive, Baltimore, MD 21218, USA*

²²*Institute of Physics, Laboratory for Galaxy Evolution, Ecole Polytechnique Federale de Lausanne, Observatoire de Sauverny, Chemin Pegasi 51, 1290 Versoix, Switzerland*

²³*Laboratory for Multiwavelength Astrophysics, School of Physics and Astronomy, Rochester Institute of Technology, 84 Lomb Memorial Drive, Rochester, NY 14623, USA*

²⁴*Department of Physics and Astronomy, Texas A&M University, College Station, TX, 77843-4242 USA*

²⁵*George P. and Cynthia Woods Mitchell Institute for Fundamental Physics and Astronomy, Texas A&M University, College Station, TX, 77843-4242 USA*

²⁶*Centro de Astrobiología (CAB), CSIC-INTA, Ctra. de Ajalvir km 4, Torrejón de Ardoz, E-28850, Madrid, Spain*

²⁷*Center for Computational Astrophysics, Flatiron Institute, 162 5th Avenue, New York, NY, 10010, USA*

²⁸*School of Astronomy and Space Science, University of Chinese Academy of Sciences (UCAS), Beijing 100049, China*

²⁹*National Astronomical Observatories, Chinese Academy of Sciences, Beijing 100101, China*

³⁰*Institute for Frontiers in Astronomy and Astrophysics, Beijing Normal University, Beijing 102206, China*

(Received n/a; Revised n/a; Accepted n/a)

Submitted to ApJL

ABSTRACT

We present the first results from the CAPERS survey, utilizing PRISM observations with the *JWST*/NIRSpec MSA in the PRIMER-UDS field. With just 14% of the total planned data volume, we spectroscopically confirm two new bright galaxies ($M_{\text{UV}} \sim -20.4$) at redshifts $z = 10.562 \pm 0.034$ and $z = 11.013 \pm 0.028$. We examine their physical properties, morphologies, and star formation histories, finding evidence for recent bursting star formation in at least one galaxy thanks to the detection of strong ($\text{EW}_0 \sim 70 \text{ \AA}$) $\text{H}\gamma$ emission. Combining our findings with previous studies of similarly bright objects at high- z , we further assess the role of stochastic star formation processes in shaping early galaxy populations. Our analysis finds that the majority of bright ($M_{\text{UV}} \lesssim -20$) spectroscopically-confirmed galaxies at $z > 10$ were likely observed during a starburst episode, characterized by a median $\text{SFR}_{10}/\text{SFR}_{100} \sim 2$, although with substantial scatter. Our work also finds tentative evidence that $z > 10$ galaxies are more preferentially in a bursting phase than similarly bright $z \sim 6$ galaxies. We finally discuss the prospects of deeper spectroscopic observations of a statistically significant number of bright galaxies to quantify the true impact of bursting star formation on the evolution of the bright end of the ultraviolet luminosity function at these early epochs.

Keywords: High-redshift galaxies (734), Early universe (435)

1. INTRODUCTION

Probing the earliest stages of galaxy formation and evolution, within the first few hundred million years of cosmic history, remains one of the greatest challenges in astronomy. These primordial galaxies have long evaded direct detection due to their intrinsic faintness and extreme redshifts. Prior to the launch of the *James Webb Space Telescope* (*JWST*), state of the art space-based facilities such as the *Hubble Space Telescope* (*HST*) and *Spitzer Space Telescope* (*Spitzer*), only managed to capture early star formation for moderate-sized samples up to $z \sim 7\text{--}8$ (e.g., Ellis et al. 2013; McLure et al. 2013; Bouwens et al. 2015; Finkelstein et al. 2015), and very small samples to ~ 11 (e.g., Oesch et al. 2016; Bouwens et al. 2021; Finkelstein et al. 2022). Detailed spectroscopic studies of rest optical/rest UV emission at these redshifts, and any further investigations at higher redshifts remained inaccessible.

Recent *JWST* observations have managed to successfully spectroscopically confirm galaxies in the early Universe, as early as $\sim 280 \text{ Myr}$ ($z = 14$) after the Big Bang (Arrabal Haro et al. 2023a; Bunker et al. 2023; Curtis-Lake et al. 2023; Carniani et al. 2024; Castellano et al. 2024; Hsiao et al. 2023; Napolitano et al. 2025; Zavala et al. 2025). While these discoveries provide an unprecedented glimpse into the emergence of the first cosmic structures, they also intensify the tension between simulations and observations. The bright ($M_{\text{UV}} \lesssim -20$) galaxies identified in these studies appear

to be unexpectedly abundant, as reflected in their contribution to the rest-frame ultraviolet luminosity function (UVLF; e.g., Finkelstein et al. 2024; Harikane et al. 2024), in stark contrast to most cosmological models calibrated before *JWST* (e.g., see Boylan-Kolchin 2023; Dayal et al. 2014; Mason et al. 2015; Behroozi & Silk 2015; Yung et al. 2019, 2020, although c.f. Lovell et al. 2021; Wilkins et al. 2023a). This, in turn, suggests that the cosmic star formation rate (SFR) density at $z > 10$ does not exhibit the rapid decline predicted by constant star formation efficiency models (Bouwens et al. 2023a,b; Harikane et al. 2023; Oesch et al. 2018), but instead follows a shallower trajectory, consistent with earlier hints from *HST* data (McLeod et al. 2016) and supported by recent *JWST* photometric samples (Donnan et al. 2023, 2024; McLeod et al. 2024; Pérez-González et al. 2023).

Several explanations have been proposed for the observed over-abundance of bright galaxies at high redshifts (for detailed discussions, see e.g., Finkelstein et al. 2024; Harikane et al. 2023, 2024; Casey et al. 2024; Franco et al. 2024). Current observations do not yet yield conclusive results on the contributions of active galactic nuclei (AGN) from galaxies at these early epochs. AGN emission, particularly from unobscured quasars, can significantly enhance observed M_{UV} , potentially inflating the estimated abundance of bright galaxies in the UVLF. Indeed, some $M_{\text{UV}} \sim -20$ sources identified at $z > 9\text{--}10$ exhibit compact morphologies accompanied by high-ionization UV spectral lines, strongly suggesting AGN activity (Bunker et al. 2023; Maiolino et al. 2023; Napolitano et al. 2024). However, an approximately equal number of similarly bright

* NASA Postdoctoral Fellow

galaxies are spatially resolved by *JWST*, displaying weak or absent AGN spectral signatures (Carniani et al. 2024; Arrabal Haro et al. 2023a,b). While AGN activity may thus account for some of these bright galaxies, this alone cannot fully explain their overall abundance.

The enhanced brightness of $z > 10$ galaxies could arise from vigorous, star-formation-driven outflows expelling dust and gas from these systems, resulting in extremely blue UV colors, nearly dust-free stellar populations, and elevated UV luminosities (Ferrara et al. 2023, 2025). Most of the currently-confirmed bright high- z galaxies (Arrabal Haro et al. 2023a; Castellano et al. 2024; Hsiao et al. 2023) indeed exhibit very blue UV slopes ($\beta \sim -2.7$) and minimal dust attenuation ($A_V \sim 0$), although with few notable exceptions (Bunker et al. 2023; Carniani et al. 2024). Still, the models outlined in Ferrara et al. (2023, 2025) require a rapid change of the dust attenuation (and thus UV colors) at $M_{UV} = -20$ between $z \sim 8$ and 11; however, the observational evidence for this is still unclear and is primarily based on photometric samples (Finkelstein et al. 2023; Papovich et al. 2023; Cullen et al. 2024).

It is also possible that a shift toward a more heavy initial mass function (IMF) can be present in these early galaxies, driven by both different chemical composition and the temperature of the cosmic microwave background (CMB) at high redshift. (Larson 1998; Bromm et al. 2002; Tumlinson 2006; Inayoshi et al. 2022; Steinhardt et al. 2023; Yung et al. 2024). Current high- z observations still cannot reliably constrain the IMF, however, as this would require deep rest-UV spectra in order to detect the signatures of massive stars such as the He II and [Ne V] lines (e.g. see Cleri et al. 2023; Chisholm et al. 2024; Katz et al. 2023; Olivier et al. 2022; Trussler et al. 2023).

Moreover, significantly reduced gas depletion timescales in early-Universe halos, facilitated by high gas densities and diminished effectiveness of feedback processes, could further enhance star formation efficiencies as indicated by the Feedback-Free Starburst model (Dekel et al. 2023; Li et al. 2024).

Future studies combining data from surveys that cover very large volumes (e.g. COSMOS-Web, COSMOS-3D) will soon offer improved constraints on this topic. If indeed these observations will be able to confirm that the bright end of the UVLF flattens out, potential drivers of this evolution could be processes that preferentially impact more massive halos, as pointed out by Finkelstein et al. (2023). Nevertheless, significant variations in star formation efficiency (SFE) or the IMF over the relatively limited dynamic range of M_{UV} and therefore

halo masses, appear unlikely (e.g. see Donnan et al. 2025).

Finally, the increase in stochasticity in the star formation histories (SFHs) of high- z galaxies could be a potential driver behind the observed trends (Sun et al. 2023; Shen et al. 2023; Muñoz et al. 2023; Gelli et al. 2024; Yung et al. 2024; Kravtsov & Belokurov 2024). Introducing some dispersion into the ratio of halo mass to UV luminosity will "upscatter" some of the numerous low-mass objects to populate the bright end of the UVLF, an effect similar to the Eddington bias. Emerging observational evidence for increased SFR variability at high- z includes spectroscopic studies of lower-mass galaxies (Looser et al. 2023), early (likely temporarily) quiescent galaxies at $z \sim 7$ (Looser et al. 2024; Weibel et al. 2024), and photometric analyses indicating recent SFH upturns in brighter galaxies at $z \sim 6$ (Ciesla et al. 2024; Endsley et al. 2024a). Despite this evidence, the current scarcity of deep *JWST*/PRISM spectroscopy—and consequently, limited emission line detections—hampers statistical analyses of SFHs in large samples of high- z galaxies.

In this work, we present initial NIRSpec spectroscopic observations of very high redshift galaxies from the CANDELS-Area Prism Epoch of Reionization Survey (CAPERS) program (PID #6368, PI: M. Dickinson). With just the first $\sim 14\%$ of the dataset collected, CAPERS has already identified two bright ($M_{UV} \sim -20.4$) galaxies at $z > 10$, increasing the known population of such objects to 12. Here we discuss the properties and SFHs of these newly discovered galaxies and combine our observations with existing studies to assess the relevance of stochastic star formation in shaping galaxy populations in the early Universe.

This paper is organized as follows. In Section 2 we present the CAPERS survey alongside the *JWST* observational data sets used in this study. In Section 3 we calculate the spectroscopic redshifts, select $z > 10$ galaxies, and discuss SED fitting and emission line measurements. In Section 4 we discuss how our results compare to the other bright galaxies spectroscopically confirmed at high- z and discuss the potential impact of bursting star formation on the enhancement of the UVLF. We summarize our findings in Section 5. Throughout this work we assume a flat Λ CDM cosmology with $\Omega_{m,0} = 0.3$, $\Omega_{\Lambda,0} = 0.7$ and $H_0 = 70 \text{ km s}^{-1} \text{ Mpc}^{-1}$, and a Chabrier (2003) initial mass function (IMF) between $0.1 - 100 M_{\odot}$. All magnitudes are expressed in the AB system (Oke 1974).

2. OBSERVATIONS AND DATA

Detailed descriptions of CAPERS target selection and prioritization, observations, data reduction, redshift measurement and spectral analysis will be presented in future publications, and are briefly summarized below.

2.1. CAPERS

CAPERS is an ongoing *JWST* Cycle 4 Treasury program of moderately deep NIRSpec multi-object spectroscopy in three fields from CANDELS (Grogin et al. 2011; Koekemoer et al. 2011) with wide-area public *JWST* NIRCам imaging: the EGS (from CEERS, PI: S. Finkelstein, Finkelstein et al. 2025), and COSMOS and UDS (from PRIMER, PI: J.Dunlop). CAPERS is obtaining low-resolution NIRSpec PRISM spectra for thousands of distant galaxies, including more than 100 candidates for objects at $z > 10$. CAPERS is building a spectroscopic legacy dataset that serves as a key resource for understanding key properties of the earliest galaxies in the Universe. In our work we focus on the first batch of CAPERS observations executed in the PRIMER-UDS field.

2.2. NIRSpec Observations

CAPERS is obtaining NIRSpec multi-object spectroscopy at seven pointing positions in each of its three survey fields. At each pointing, CAPERS normally observes three configurations of the NIRSpec Micro-Shutter Assembly (MSA) with a common pointing center and position angle, each with an effective exposure time of 5690 s (1.58 h). This scheme allows for faint and high-priority targets to be repeated in multiple configurations and thus receive total exposure times up to 17069 s (4.74 h). Most other targets are changed between subsequent MSA configurations, replaced with new targets to maximize the total object yield.

The CAPERS UDS observations were scheduled between UT 31 December 2024 and 10 January 2025. Two of the 21 planned MSA observations failed due to technical issues with the spacecraft, and 13 more were canceled due to communication restrictions with *JWST* during the Los Angeles area wildfires in January. Only one UDS pointing was observed using all three planned MSA configurations. Two pointings were observed in two out of three planned MSA configurations, and a final pointing was observed with only one MSA configuration. The remaining three pointings in UDS have not yet been observed.

Altogether, about 1200 individual targets were observed in these first 8 UDS MSA configurations. The full details of the target selection, prioritization, and MSA planning will be given in a forthcoming paper. For each MSA configuration, these observations employed a 3-shutter slitlet nod pattern at an aperture position angle

(APA) of approximately 201° . Sources were correspondingly assigned 3 shutter slitlets and source-source spectral overlap was avoided whenever possible. Each of the six nods was observed for a single 13 group integration using the NRSIRS2 readout pattern.

2.3. NIRSpec Data Reduction and Calibration

We use the CAPERS team internal data reduction in this work. This reduction largely uses the standard *JWST* pipeline¹ (Bushouse et al. 2024) version 1.16.1 and CRDS version 1312.pmap with a few modifications, which include the removal of the $1/f$ noise from the exposures and a modified flat-field file during the `calwebb_spec2` stage (see Arrabal Haro et al. 2023a,b, for more detail). Observations in three of the UDS pointings incorporated small ($\pm 0.05''$) cross-dispersion dithers between two nod sequences to test potential benefits for outlier rejection and mitigation of artifacts and correlated noise. These dithers require some additional attention in the pipeline processing. Finally, we run `calwebb_spec3` to combine data from the nods and produce our final data products. One-dimensional spectra were extracted for 1196 sources, including both ‘boxcar’ and optimally-weighted extractions for most objects.

Additionally, for sources in slits with compact companions, an alternative nodding pattern was employed, limiting the nodded exposures that are combined in such a way that the shutter containing the contaminant companion is never subtracted from the shutter hosting the primary source. This implies that the background is estimated from fewer shutters in some exposures, but it does not diminish the effective integration time on the source of interest. The result is an asymmetric nodding pattern that avoids oversubtraction in the region of the 2D spectra corresponding to the central source.

2.4. Photometry

We make use of photometry to select targets for NIRSpec observation, and during our spectroscopic modeling below, both to constrain the overall shape of the spectral energy distribution (SED), and to correct for NIRSpec slit losses. Our photometric process predominantly follows that described in detail in Finkelstein et al. (2024), thus we direct the reader there for more details. For our photometry we use NIRCам and MIRI F770W mosaics provided by the PRIMER team. We use Source Extractor (Bertin & Arnouts 1996) to detect sources in a weighted sum of the F277W and F356W images, and to measure photometry in all seven NIRCам bands available from the PRIMER survey (PID

¹ <https://github.com/spacetelescope/jwst>

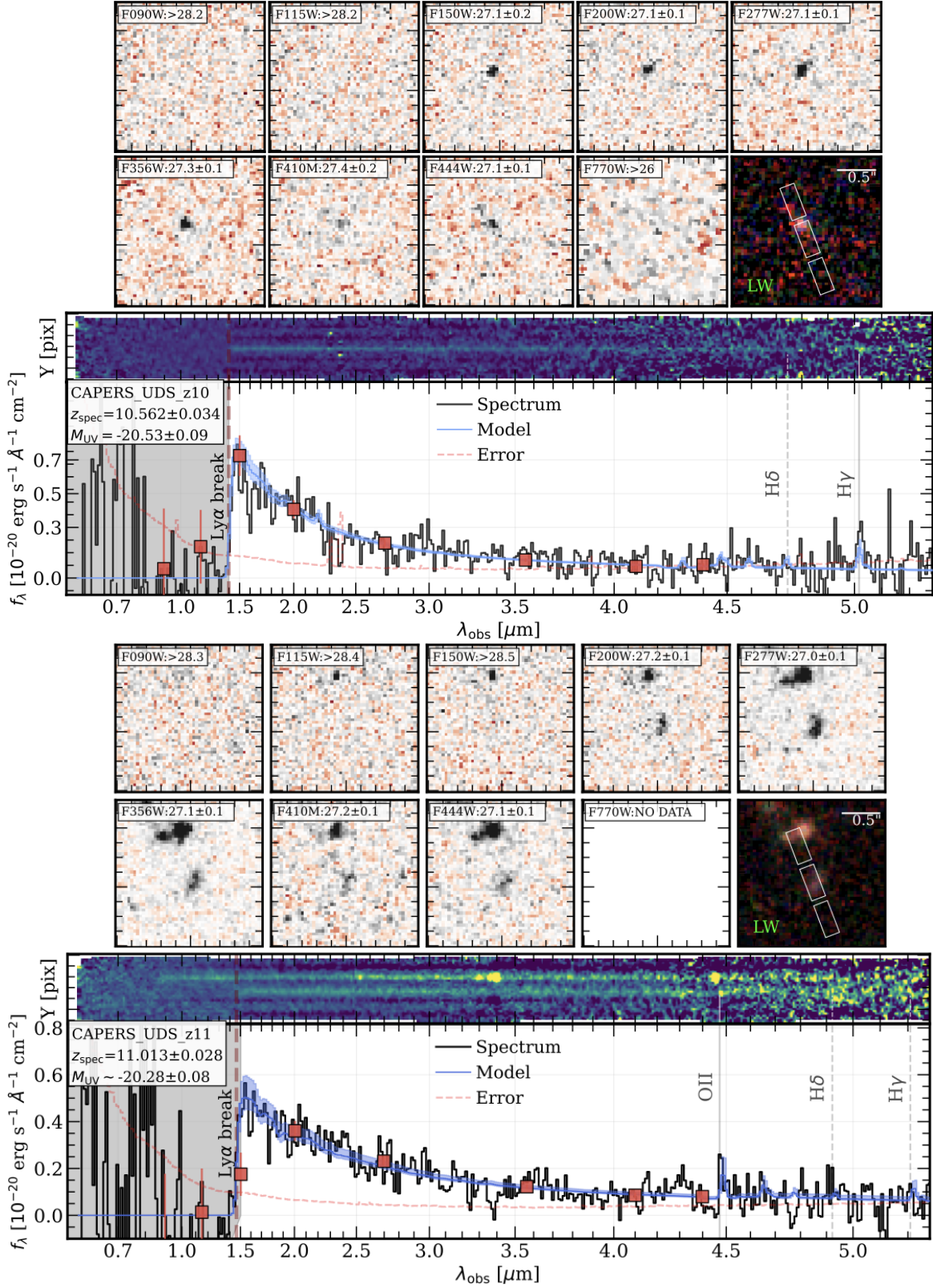


Figure 1. CAPERS high- z sources. **Top:** *JWST*/NIRCam and MIRI F770W 2'' image stamps and RGB long wavelength color images comprised of the F277W, F356W, and F444W bands, respectively. The MSA slitlet layout (white) is overlaid on the LW image. Each panel shows the total magnitude as presented in the photometric catalog. The spectrum of CAPERS_UDS_z11 was processed with an alternative nodding pattern (see end of Section 2.3), to remove the impact of the companion source on the final spectrum. **Middle:** 2D MSA PRISM spectrum. **Bottom:** 1D spectra of CAPERS galaxies in the observed frame. We show the spectroscopic data in black, while the 1σ uncertainty on the spectrum is in dashed red. Best-fit BAGPIPES model is shown in solid blue, with its uncertainty highlighted by a shaded region. NIRCam photometry is shown with square symbols. Further, we show the positions and label the prominent emission with significant ($> 3\sigma$) detections as solid vertical lines. Emission lines for which we only obtain an upper limit are shown with dashed lines.

1837, PI: J.Dunlop), as well as MIRI F770W (also from PRIMER), and archival *HST*/ACS imaging including the F435W band from PID 16872 (PI: N.Grogin) and the F606W and F814W bands from CANDELS (Grogin et al. 2011; Koekemoer et al. 2011). Photometry is measured using small Kron apertures, corrected to total based both on the ratio between the flux in a small Kron and a larger Kron aperture in the F277W image, and a simulation-based residual aperture correction. Sources are originally identified in a “cold” mode run, with fainter, smaller sources in a more aggressive “hot” mode run added in if they were not included in the segmentation map of the cold run (see e.g. Rix et al. 2004). Prior to photometry, images with smaller PSFs than the F277W image are convolved with an empirically derived PSF kernel to match the F277W PSF; for larger-PSF images, the photometry is measured without convolution but a correction is derived from the ratio of the flux in the F277W image convolved to the PSF of the larger image to the native F277W image. Photometric redshifts are measured with EAZY (Brammer et al. 2008), using the provided FSPS templates combined with the updated templates of Larson et al. (2023).

3. DATA ANALYSIS

3.1. Spectroscopic Redshifts

The CAPERS team is using a variety of software codes plus interactive inspection and vetting to measure redshifts from the NIRSpec spectra, as will be described in detail in a future paper. The present analysis employed an initial review of all 1196 extracted spectra using a modified version of MSAEXP² (Brammer 2022; Kokorev et al. 2024a). Our procedure first fits a linear combination of EAZY (Brammer et al. 2008) models, specifically the BLUE_SFH_Z13 model subset³ that contains redshift-dependent SFHs, and dust attenuation values. These models are further complemented by a blue galaxy template, derived from a *JWST* spectrum of a $z = 8.50$ galaxy with extreme line equivalent widths (Carnall et al. 2022). Once we obtain an initial $p(z)$ from the template fitting we perform a second MSAEXP pass on the sources by fitting sets of Gaussian continuum splines and emission lines templates to our spectrum. As an input parameter, we set `nsplines=11` and allow to search for the minimal χ^2 value across the prior range set by the template fitting. We leave the position, amplitude and width of emission lines as free

parameters, with the latter allowed to vary between 150 – 800 km/s. The uncertainty is derived via MCMC by resampling the covariance matrix. In these fits we have used the spectra corrected to the photometry discussed in Section 2.4. Further, the PRISM dispersion curve is convolved with the input models prior to the fit to account for the wavelength dependent spectral resolution.

Our two-fold approach is especially effective when the number of significantly detected emission lines is limited, like at high redshift, and allows us to constrain the redshift via the break first, and then to refine it and further extract all available information about the emission features in the second pass.

3.2. Selection of $z > 10$ Objects

Finally, we select high- z ($z > 10$) galaxies from the spectra. Out of 22 $z > 10$ candidates placed on the MSA shutters in this first batch of CAPERS-UDS data, we only identify two objects where the high- z nature can be securely confirmed. The analysis of the remaining spectra (also see Section 2.2 regarding failed/canceled observations) is still ongoing, and will be presented in the full CAPERS overview paper once the full data-set is available. (M. Dickinson in prep.).

Initially, CAPERS_UDS_z10 (ID:136645) and CAPERS_UDS_z11 (ID:126973) were identified at $z_{\text{phot}} \simeq 9.97$ and $z_{\text{phot}} \simeq 11.95$ via the EAZY photometric fitting. The two objects were observed between January 1st and 9th 2025. In Figure 1 we show the shutter positions overlaid on $2''0$ cutouts of the high- z sources. To mitigate the contamination from a low- z source in one of the CAPERS_UDS_z11 slitlets, we only combine the nodded exposures in a way that the contaminant is never subtracted from the spectrum of the primary source, as described in Section 2.3. Both of the objects presented in this work were each observed in two MSA configurations for a total of 11379s each. Further, we do not observe strong emission lines detected at high significance in either object, however a clear Ly α break present in both sources allows us to securely derive a redshift of $z_{\text{spec}} = 10.56 \pm 0.04$ for CAPERS_UDS_z10 and $z_{\text{spec}} = 11.00 \pm 0.04$ for CAPERS_UDS_z11.

3.3. Emission Lines

Both spectra exhibit prominent Ly α breaks at $\lambda_{\text{rest}} \simeq 1216 \text{ \AA}$, which are clearly visible in both the 1D and 2D spectra (Figure 1) with a high level of significance. There is no indication of Ly α emission, as has been reported in a handful of other $z > 10$ galaxies (Bunker et al. 2023; Curtis-Lake et al. 2023; Witstok et al. 2024), though the resolution of the prism prohibits detection of faint emission lines at the blue end of the spectrum.

² <https://github.com/VasilyKokorev/msaexp-OLF>

³ <https://github.com/gbrammer/eazy-photoz/tree/master/templates/sfhz>

To further investigate the spectral properties of these galaxies, we conducted a detailed inspection of both the 1D and 2D PRISM spectra, searching for prominent emission lines above the noise level. To do that we use the 1D Gaussian MSAEXP fits to our spectra. Despite a $\sim 3\sigma$ detection of the continuum in both objects across the majority of the spectrum, we identify only two emission lines: a significant ($> 4\sigma$) detection of $H\gamma$ in CAPERS_UDS_z10, and a $\sim 5\sigma$ $OII - 3727 \text{ \AA}$ line in CAPERS_UDS_z11. From both lines we are thus able to measure more precise spectroscopic redshifts of $z_{\text{spec}} = 10.562 \pm 0.034$ and $z_{\text{spec}} = 11.013 \pm 0.028$, respectively, fully consistent with our previous measurement from the $Ly\alpha$ break. We will adopt line redshifts for both sources throughout our work. With MSAEXP we measure the rest-frame equivalent width (EW_0) of the detected $H\gamma$ in CAPERS_UDS_z10 at $74 \pm 18 \text{ \AA}$.

The second object, CAPERS_UDS_z11, appears devoid of any significantly detected Balmer lines. The absence of strong spectral features is not unexpected at high redshifts, as the strong emission lines such as the $[OIII]$ doublet and $H\beta$ shift out of the NIRSpect wavelength coverage ($\gtrsim 5.3 \mu\text{m}$). This leaves us only with higher order (and fainter) Balmer lines and typically-weak metal lines in the observed spectrum range. For instance, the current record-breaking high- z galaxies presented in Carniani et al. (2024) also exhibit a lack of prominent emission lines in the rest-optical for that reason. In addition, the expected position of the $H\gamma$ line at $z \sim 11$ would fall into a much noisier part of the spectrum, further complicating its detection. We, however, do observe an OII line at $EW_0 = 47 \pm 10 \text{ \AA}$ in this object, although given the shape of this line and its proximity to a trough in the continuum the true SN of this feature is likely below 5. Further, we also derive upper limits on the flux and EW_0 of both $H\delta$ and $H\gamma$ for CAPERS_UDS_z11. We report the detected emission line fluxes, EW_0 and upper limits in Table 2.

3.4. SED Fitting

So far we have used MSAEXP to measure spectroscopic redshifts as well as the intensities of the few spectral lines we have detected. We have noted that the strong $H\gamma$ line in CAPERS_UDS_z10 could indicate that the galaxy light is dominated by a burst of star formation (e.g. see Leitherer et al. 2014). To test this hypothesis we perform stellar population modeling with the SED fitting code BAGPIPES (Carnall et al. 2018, 2019), which simultaneously models both the photometry and full spectrum to constrain a variety of physical properties, including the star-formation history.

Table 1. CAPERS UDS high- z sample.

Parameter	CAPERS_UDS_z10	CAPERS_UDS_z11
RA [deg]	34.456023	34.264439
Dec [deg]	-5.121952	-5.096232
z_{spec}	10.562 ± 0.034	11.013 ± 0.028
M_{UV} [AB mag]	-20.53 ± 0.09	-20.28 ± 0.08
R_{eff} [pc]	420 ± 70	560 ± 61
BAGPIPES FIT		
β	-2.27 ± 0.12	-1.71 ± 0.12
SFR ₁₀ [M_{\odot}/yr]	18 ± 5	43 ± 10
SFR ₁₀₀ [M_{\odot}/yr]	9 ± 5	22 ± 5
$\log_{10}(\text{SFR}_{10}/\text{SFR}_{100})$	0.3 ± 0.2	0.3 ± 0.5
$\log_{10}(M_{*}/M_{\odot})$	8.3 ± 0.2	8.7 ± 0.2
A_V	0.31 ± 0.10	0.74 ± 0.11
Age [Myr]	< 18	< 20
EMPIRICAL		
SFR ₁₀ [M_{\odot}/yr]	43 ± 10	< 80
SFR ₁₀₀ [M_{\odot}/yr]	20 ± 3	43 ± 5
$\log_{10}(\text{SFR}_{10}/\text{SFR}_{100})$	0.3 ± 0.1	< 0.3

We adopt a non-parametric star-formation history (SFH) with the ‘bursty continuity’ prior from Tacchella et al. (2022), using eight time bins where the SFR is fit to a constant value in each bin. The first four bins are set to lookback times of 0-3 Myr, 3-10 Myr, 10-30 Myr, and 30-100 Myr, while the last four bins are logarithmically spaced between 100 Myr and $t_{\text{max}} = t_{\text{universe}}(z = z_{\text{spec}}) - t_{\text{universe}}(z = 20)$. We fixed the redshift at the spectroscopic redshift to remove any photometric uncertainties that may propagate into the SED fitting. Dust attenuation is assumed to follow the Calzetti et al. (2000) law and the rest-frame V-band attenuation is fit (log-uniform prior) in the range $A_V = 0.001 - 3 \text{ mag}$. Stellar nebular emission is included with an ionization parameter in the range $-4 \leq \log U \leq 0$. Our $\log U$ upper limit was chosen to accommodate galaxies with high ionization values, as is common at high redshift (e.g. see Carnall et al. 2022). We allow for an intrinsic stellar velocity dispersion in the range 50–500 km/s, though we provide the BAGPIPES fits with the NIRSpect PRISM dispersion curve to convolve the resolution of the BAGPIPES models to the resolution of the input spectral data. The metallicity is allowed to vary between $0.001 - 1 Z_{\odot}$ (log-uniform prior for both). To account for differences between the spectra and photometry due to slit losses, we incorporate parameters into the BAGPIPES fitting that handle the modeling of noise and the calibra-

tion to the photometry using the prescription outlined in [Carnall et al. \(2019\)](#).

To test other star formation history models we repeat the same procedure but this time restrict the burstiness parameter in the non-parametric SFH model to be strictly positive, replicating a rising SFH. We also tested a declining SFH by adopting an exponential SFH model. The parameter bounds for the dust and nebular priors are exactly the same as the non-parametric SFH. The bounds for the exponential SFH parameters are: a uniform prior of age to be 0.001–1 Gyr, uniform prior in τ to be 0.002–11, a \log_{10} prior for metallicity ranging between 0.001–1 Z_{\odot} . The posteriors and SFHs for our galaxies are presented in [Figure 2](#) and [Figure 3](#).

From the BAGPIPES modeling, we find that CAPERS_UDS_z10 is well characterized by a rising non-parametric SFH ($\Delta\chi^2 > 3.0$ compared to declining SFH model), indicative of a current starburst. This conclusion is supported by the ratio of SFRs measured over the recent 10 Myr (SFR_{10}) and 100 Myr (SFR_{100}) timescales, which yields $\log_{10}(\text{SFR}_{10}/\text{SFR}_{100}) \sim 0.3$ (which is consistent with the value derived directly from the spectrum, as will be discussed in [Section 3.5](#)). The object also exhibits a relatively blue UV spectral slope ($\beta \sim -2.27$) and a modest level of dust obscuration ($A_V \sim 0.3$ mag).

In contrast, results for the second object, CAPERS_UDS_z11, are less definitive. The non-parametric model prefers a recent burst, similarly to the first galaxy, however the uncertainty on the fit is larger due to a lack of securely detected Balmer lines. To test the validity of this fit, we check the alternative SFH parameterizations fit to this object and find that the data are non-parametric SFH is marginally ($\Delta\chi^2 \sim 1 - 2$) preferred, compared to the rising and exponentially declining star formation histories. This ambiguity arises primarily due to the lack of Balmer series lines, limiting our ability to constrain the recent star formation history reliably. We reflect this in our uncertainty on the measurement where we find $\log_{10}(\text{SFR}_{10}/\text{SFR}_{100}) = 0.3 \pm 0.5$. With the current data, it remains uncertain whether CAPERS_UDS_z11 is undergoing a recent burst, or is “napping” in a period of temporary quiescence following a burst (e.g. [Looser et al. 2024](#); [Cole et al. 2025](#)).

Additionally, CAPERS_UDS_z11 is notably redder ($\beta \sim -1.7$) compared to CAPERS_UDS_z10 with a BAGPIPES fit implying a higher dust attenuation ($A_V \sim 0.7$ mag). These properties are consistent across all SFH scenarios we explore. A summary of all derived physical parameters from our BAGPIPES analysis is provided in [Table 1](#).

3.5. Empirical UV Properties

We estimate the absolute UV magnitude for each galaxy from the photometry-calibrated spectrum at $\lambda_{\text{rest}} \sim 1500$ Å, and find that our targets have $M_{\text{UV}} = -20.53 \pm 0.09$ for CAPERS_UDS_z10 and $M_{\text{UV}} = -20.35 \pm 0.08$ for CAPERS_UDS_z11. On top of deriving the UV-slope β with BAGPIPES, we also compute it by assuming $f_{\lambda} \sim \lambda^{\beta}$ and deriving it directly from the spectrum within the $\lambda_{\text{rest}} = 1250\text{--}3000$ Å range. From the photometry corrected spectra we directly measure $\beta = -2.26 \pm 0.11$ and $\beta = -1.90 \pm 0.12$ for CAPERS_UDS_z10 and CAPERS_UDS_z11, respectively, fully consistent with the β values already derived with BAGPIPES, within $< 1\sigma$.

As a check on the derived $\text{SFR}_{10}/\text{SFR}_{100}$, we perform an independent empirical estimation based on emission line fluxes (or their upper limits) and the UV magnitude (M_{UV}). We assume Case B recombination conditions, adopting intrinsic line ratios of $(\text{H}\alpha/\text{H}\gamma)_{\text{int}} \sim 6.1$ and $(\text{H}\alpha/\text{H}\delta)_{\text{int}} \sim 10.6$ ([Osterbrock 1989](#)). Using the dust attenuation derived from BAGPIPES, we correct the observed line fluxes (or upper limits) to estimate the intrinsic $\text{H}\alpha$ luminosity, and convert the observed M_{UV} to the intrinsic one. So far, there are only 3 direct $\text{H}\alpha$ detections at $z > 10$, so we can attempt to directly compare our Case B converted luminosities to them. We find that our dust-corrected $\text{H}\alpha$ luminosities are $L_{\text{H}\alpha} \sim 6 \times 10^{42}$ erg/s for CAPERS_UDS_z10 and an upper limit $L_{\text{H}\alpha} \lesssim 6 \times 10^{42}$ erg/s for CAPERS_UDS_z11. Interestingly, comparing the $L_{\text{H}\alpha}$ to the existing high- z samples, we find a value that is $\times 5$ higher than that in MACS0647-JD ([Hsiao et al. 2024](#)), and is much more comparable to GHZ2 ([Zavala et al. 2025](#)) and GNz11 ([Álvarez-Márquez et al. 2024](#)). We will expand on it further in [Section 4.3](#). Finally, our intrinsic $\text{H}\alpha$ luminosities and the M_{UV} are then converted to SFR_{10} and SFR_{100} , respectively, following the relations provided by [Kennicutt \(1998\)](#).

From the detected $\text{H}\gamma$ emission line in CAPERS_UDS_z10, we empirically determine $\log_{10}(\text{SFR}_{10}/\text{SFR}_{100}) = 0.3 \pm 0.1$, fully consistent with the BAGPIPES result. For CAPERS_UDS_z11, neither $\text{H}\gamma$ nor $\text{H}\delta$ lines are detected, limiting our estimate to an upper bound on SFR_{10} . Given that the expected $\text{H}\gamma$ line position lies too close to the upper observed wavelength limit of the PRISM, we adopt the $\text{H}\delta$ flux upper limit ([Table 2](#)) to constrain the SFR_{10} . This yields $\log_{10}(\text{SFR}_{10}/\text{SFR}_{100}) < 0.3$, which is consistent with, albeit lower than the limit derived by BAGPIPES.

3.6. Size Measurements

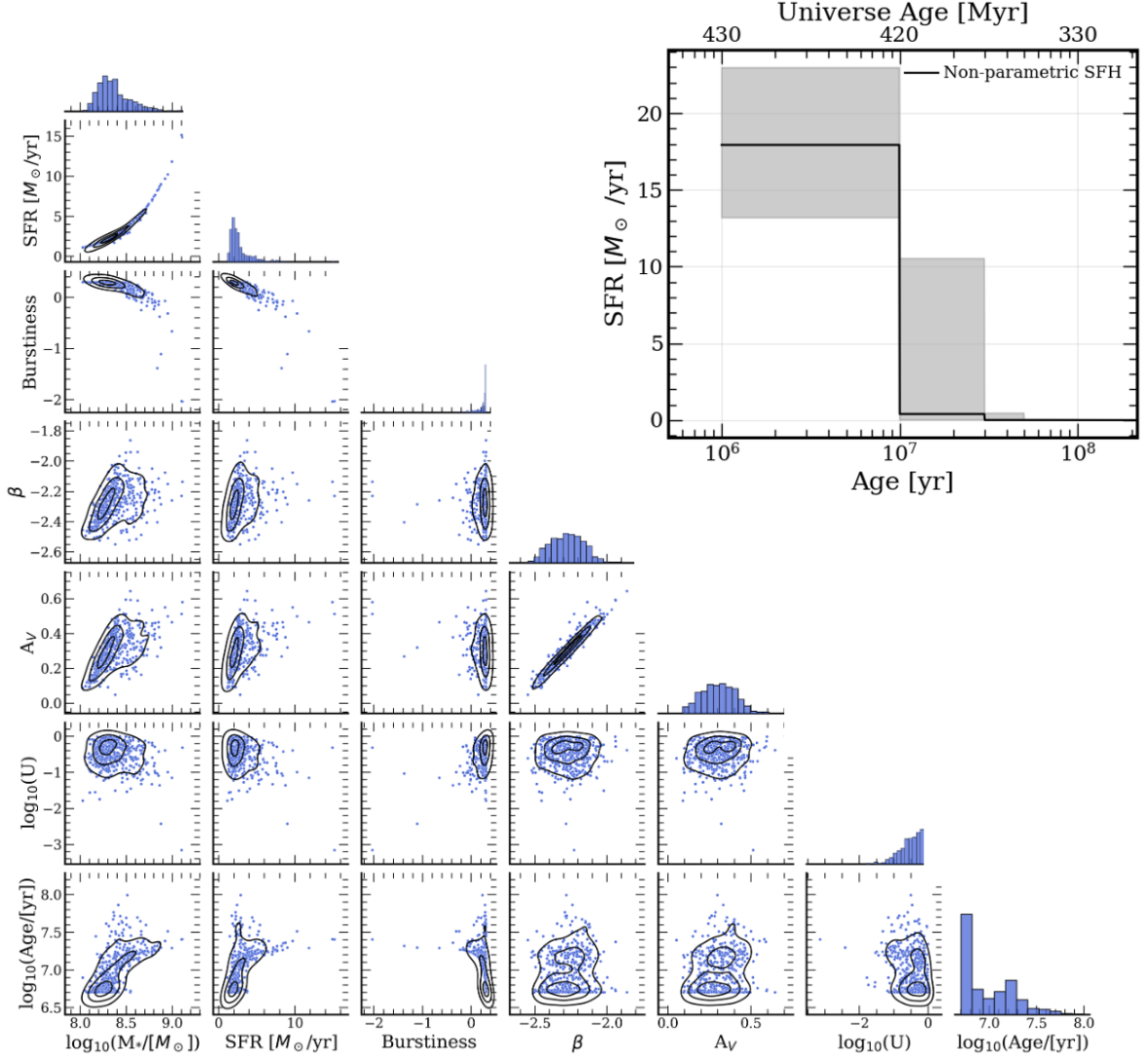


Figure 2. BAGPIPES Posteriors and SFH for CAPERS_UDS_z10. **Left:** Posterior probability distributions obtained with BAGPIPES for the non-parametric SFH fit. The columns (left to right) show the M_* , SFR_{100} , Burstiness (defined as $\log_{10}\text{SFR}_{10}/\text{SFR}_{100}$), UV slope β , dust extinction A_V , ionization parameter $\log_{10}U$ and the mass weighted age. We plot the 1D posterior distributions of each parameter along the diagonal. On 2D scatter plot we show the joint posterior distributions with contours representing the 1, 2 and 3σ intervals. **Right:** The best-fit non-parametric SFH. The shaded region shows the $\pm 1\sigma$ uncertainty on the fit.

Cutouts presented in Figure 1 show that while our sources are compact they are still clearly resolved. We measured the effective radius (R_{eff}) to compare the sizes of CAPERS $z > 10$ galaxies to other galaxies at similarly early epochs, modeling the galaxies with GALFIT (Peng et al. 2002, 2010). When fitting we take into account the effects of the PSF, which we have measured empirically from the bright stars in the field. The same PSFs were also used when constructing the photometric catalog described in Section 2.4. We model the object with a Sérsic (Sérsic 1963) profile where the source posi-

tion, brightness, effective radius, Sérsic index, and axis ratio are allowed to vary.

We perform this procedure on our highest SNR band, F277W, to ensure optimal S/N per pixel is achieved to accommodate robust size measurements, a procedure often employed for other $z > 10$ galaxies (e.g. see Arrabal Haro et al. 2023a; Kokorev et al. 2024b). Moreover, while the F277W band has a $\times 2$ poorer resolution compared to the F200W, the higher S/N (per pixel) in the LW band means that extended structure can be detected and modeled in a more robust way. We find that the on-the-sky sizes of our sources are $R_{\text{eff}} = 0.10 \pm 0.02''$

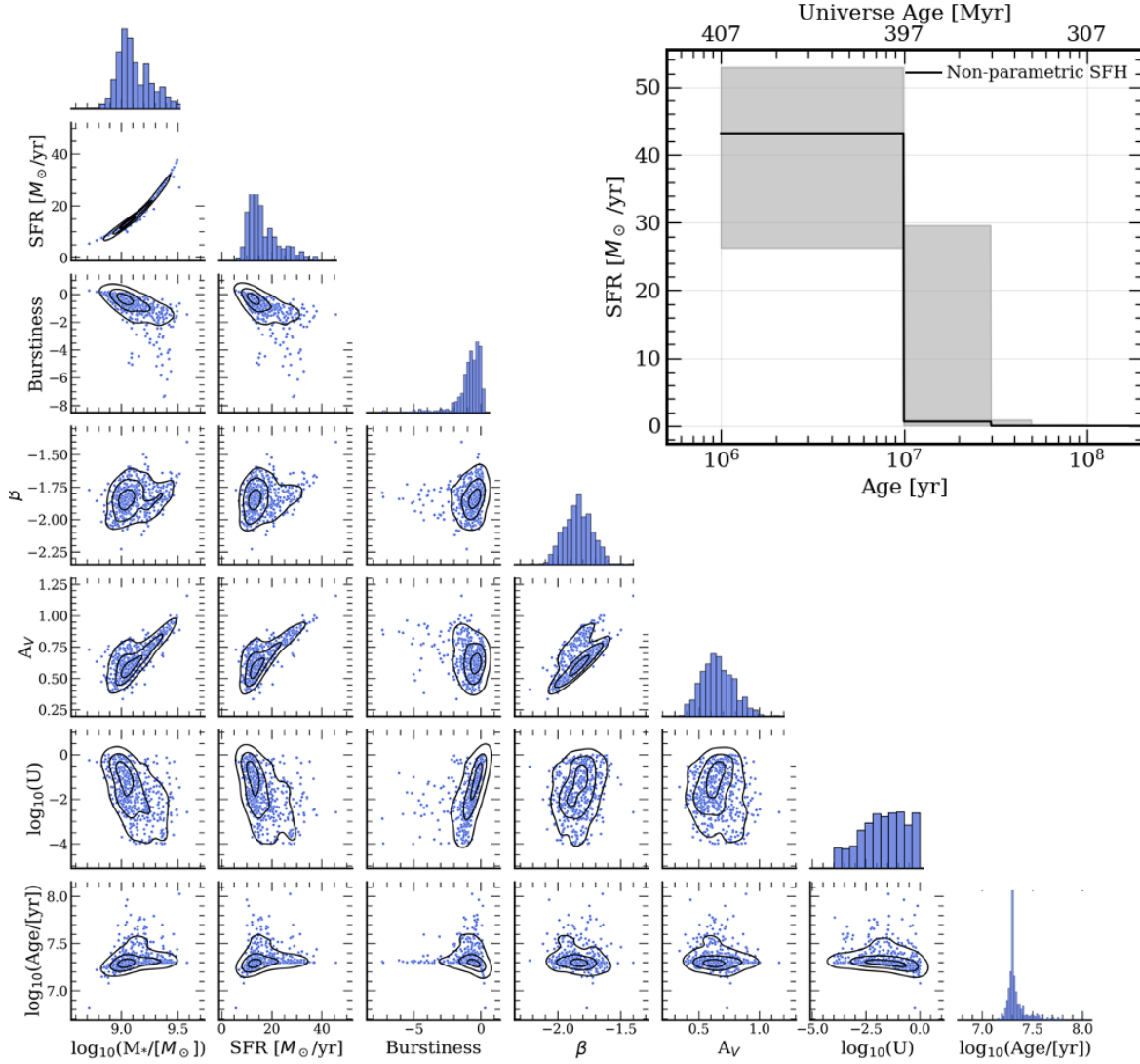


Figure 3. BAGPIPES Posteriors and SFH for CAPERS_UDS_z11. Same as Figure 2.

for CAPERS_UDS_z10 and $R_{\text{eff}} = 0.14 \pm 0.02''$ for CAPERS_UDS_z11. Both of our sources appear to be resolved, with CAPERS_UDS_z11 in particular showing potential signs of interactions/merger. Taking the redshift into account, we convert our angular sizes to physical effective radii. We obtain $R_{\text{eff}} = 420 \pm 70$ pc for CAPERS_UDS_z10 and $R_{\text{eff}} = 460 \pm 61$ pc CAPERS_UDS_z11. These sizes are also listed in Table 1.

4. RESULTS AND DISCUSSION

4.1. Stellar Population Properties

While only observed with modest (~ 3.2 hours) integration times, these targets are sufficiently bright to be detected at $> 3\sigma$ level across all spectral pixels. While this, plus the detection of certain emission line features, is perfectly adequate to constrain the redshift, properties

of the most recent episode of star formation, such as UV-slope, age and dust obscuration, deriving any further physical parameters such as stellar mass or metallicity would not be reasonable due to the lack of rest-optical continuum and a sufficient number of detected emission lines. As such, we will only focus on stellar population parameters that can be derived from the rest-UV alone.

We find that both of our objects are bright, with a median $M_{\text{UV}} \sim -20.4$, therefore confirming these two CAPERS galaxies at $z = 10.562$ and $z = 11.013$, which raises the number of UV-bright ($M_{\text{UV}} \sim -20$) galaxies at $z > 10$ to a total of 12 (Arrabal Haro et al. 2023a,b; Castellano et al. 2024; Carniani et al. 2024; Hsiao et al. 2023, 2024; Oesch et al. 2016; Bunker et al. 2023; Maiolino et al. 2023; Napolitano et al. 2025; Fujimoto et al. 2024). We now would like to explore what

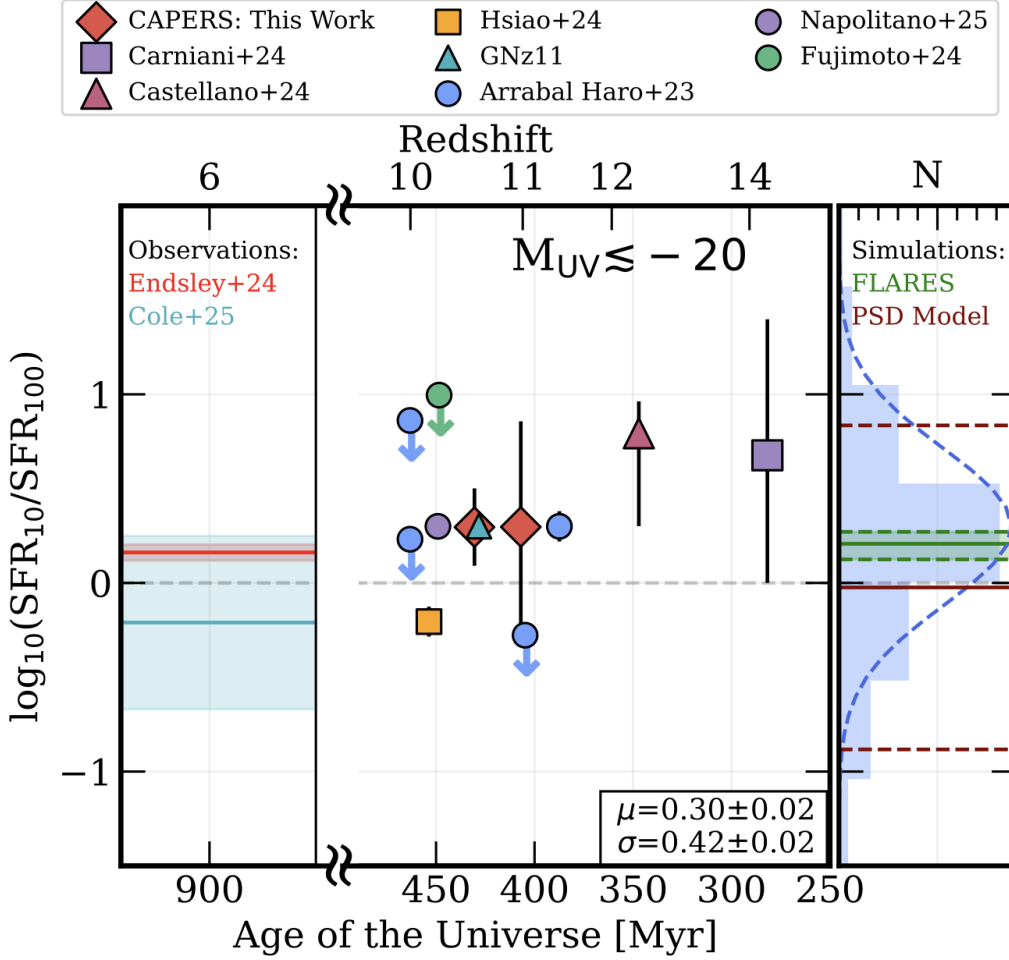


Figure 4. Bursting Star Formation of bright of $z > 10$ galaxies. The ratio between SFR_{10} and SFR_{100} as a function of the age of the Universe. Alongside the CAPERS (red) galaxies, we show all the literature results for $M_{UV} < -20$ high- z galaxies which report on the recent SFR (Carniani et al. 2024; Hsiao et al. 2023, 2024; Bunker et al. 2023; Álvarez-Márquez et al. 2024; Fujimoto et al. 2024; Napolitano et al. 2025). The CEERS high- z galaxies presented in (Arrabal Haro et al. 2023a,b), and bright $z \sim 10$ galaxies presented in Napolitano et al. (2025) and Fujimoto et al. (2024) do not report SFR_{10} , and were thus fit with the same BAGPIPES set-up as discussed in Section 3.4. In the right panel we show burstiness distribution created by MCMC resampling all the available data. The dashed blue line shows the best-fit Gaussian to the burstiness distribution, with the best-fit mean (μ) and standard deviation (σ) listed in the inset panel. We additionally show results from the PSD toy model (maroon) and hydrodynamical simulations (FLARES; Lovell et al. 2021; Wilkins et al. 2023b,c, in green) of burstiness at high- z . Finally, in a subpanel on the left we show medians (solid lines) and 68 % confidence intervals (shaded regions) of observational constraints on burstiness of bright $z \sim 6$ galaxies from Endsley et al. (2024b) and Cole et al. (2025).

other similarities, apart from brightness and their high- z nature, and any significant differences these objects have.

It does appear that while dust attenuation, as derived by BAGPIPES, is low, it is not negligible. For CAPERS_UDS_z10 we find $\beta \simeq -2.27$ and $A_V \simeq 0.3$ which exactly match the ones observed in JADES-GS-z14-0 (Carniani et al. 2024), assuming that the Calzetti et al. (2000) attenuation law is valid at high redshift (used in other high- z galaxy works e.g. Carniani et al. 2024). Further, the BAGPIPES fit includes nebular continuum so it is unlikely that the reddening we derive is being

artificially induced. While we report no UV lines in CAPERS_UDS_z10, Carniani et al. (2024) find a tentative C III] line for JADES-GS-z14-0. Given that our object is ~ 0.3 mags fainter, it is likely that the S/N of our spectrum is not sufficiently high. On the other hand, CAPERS_UDS_z11 has a notably shallower UV slope - $\beta \simeq -1.71$ and consequently a larger $A_V \sim 0.74$. If true, this would make it one of the dustiest high- z galaxies observed by *JWST*, and could in part explain the lack of emission lines. It is worth noting that we still lack data beyond $\lambda_{\text{rest}} \sim 4000 \text{ \AA}$, and therefore constraining dust attenuation solely relies on the UV slope. Moreover, a

lack of detection of typical metallicity-constraining lines further complicates a robust estimate of A_V . Further observations of the dust continuum in the CAPERS (and other) high- z galaxies with e.g. ALMA would be needed to more accurately constrain their dust content.

Finally, it is also worth noting that while both of the objects presented in this work are UV luminous, their significant level of dust attenuation shows that bright galaxies at $z \gtrsim 10$ can be somewhat attenuated (c.f. see [Mitsuhashi et al. 2025](#)), casting doubt on feedback-based dust removal as the only cause of the high bright end of the UVLF (e.g. [Ferrara et al. 2023](#)).

4.2. Compact and Extended Galaxies at $z > 10$

We further compare our measured effective radii with empirically derived sizes of spectroscopically confirmed galaxies at $z > 10$, as well as predictions derived from extrapolating scaling relations established at lower redshift. The two galaxies examined in our analysis exhibit extended morphologies, characterized by effective radii of approximately $R_{\text{eff}} \sim 500$ pc. In addition CAPERS.UDS.z11 appears to have multiple components and faint extended features, likely hinting at its interacting/merging nature (and more tentatively also CAPERS.UDS.z10). These measurements align closely with those observed in the similarly luminous ($M_{\text{UV}} < -20$) high-redshift galaxy sample from CEERS, as recently presented by [Arrabal Haro et al. \(2023a,b\)](#). Furthermore, the sizes of CAPERS galaxies are consistent within roughly 1σ uncertainty with the current record holder for highest confirmed spectroscopic redshift—JADES-GS-z14-0 ([Carniani et al. 2024](#)).

Interestingly, extended morphology does not universally characterize luminous galaxies at these early epochs. Objects such as GNz11 ([Oesch et al. 2016](#); [Maiolino et al. 2023](#); [Bunker et al. 2023](#)) and GHZ2 ([Castellano et al. 2024](#); [Ono et al. 2023](#); [Yang et al. 2022](#)) are significantly more compact, with radii constrained to $R_{\text{eff}} \lesssim 100$ pc. This striking contrast in morphologies among similarly bright, early-universe galaxies raises important questions: Does the morphological diversity observed at these extreme redshifts provide insights into the underlying mechanisms driving their remarkable UV luminosities? Can the differences in galaxy sizes and structures illuminate pathways governing their early evolutionary histories?

While a statistical census of ionization properties and sizes at high redshift remains limited by data volume, emerging evidence points to possible physical drivers behind observed trends. The presence of high-ionization UV lines in compact objects may be driven by AGN activity or extremely compact star formation ([Álvarez-](#)

Table 2. Emission Line Properties.

ID	O II 3727 Å	Hδ 4101.7 Å	Hγ 4340.4 Å
Line Flux [10^{-20} erg s $^{-1}$ cm $^{-2}$]			
UDS.z10	—	—	54.6 ± 14.0
UDS.z11	37.2 ± 7.3	< 24	< 20
Rest Frame EW [Å]			
UDS.z10	—	—	74 ± 18
UDS.z11	46 ± 10	< 19	< 10

[Márquez et al. 2024](#); [Castellano et al. 2024](#); [Zavala et al. 2025](#)). In contrast, the enhanced brightness of extended galaxies at $z > 10$ may result from high star formation efficiency and/or stochastic star formation potentially triggered by mergers—similar to what is observed in $z \sim 7$ systems ([Harikane et al. 2024](#)).

Theory predicts higher merger rates in the early Universe (e.g. [Fakhouri et al. 2010](#); [Rodríguez-Gomez et al. 2015](#)) compared to those at $z \sim 6 - 7$. Moreover, major merger timescales at high redshift are shorter than the age of the Universe, which, as [Harikane et al. \(2024\)](#) argue, may imply that most M_{UV} -bright galaxies have undergone at least one such event.

The galaxies presented in this study exhibit extended morphologies and notably distinct spectral features compared to compact high- z objects, which typically display stronger UV emission lines. We specifically would like to note signs of potential interactions/mergers present in both objects, particularly in CAPERS.UDS.z11 which exhibits two distinct clumps in [Figure 1](#). Currently however, fully characterizing the relationship between galaxy sizes and UV line intensities at $z > 10$ remains challenging due to limited sample sizes. Addressing this gap is one of the primary objectives of the CAPERS survey, which is anticipated to deliver tens of additional high- z galaxy spectra upon completion, significantly advancing our understanding of how early galaxy properties affect their morphology, and vice-versa.

4.3. Bursting Star Formation

We will now explore how prevalent bursting star formation is at the bright end ($M_{\text{UV}} < -20$) of the high- z UVLF. To achieve this, we complement our derived burstiness metric, $\log_{10}(\text{SFR}_{10}/\text{SFR}_{100})$, with similarly luminous galaxies reported in the literature showing evidence of bursting star formation ([Álvarez-Márquez et al. 2024](#); [Bunker et al. 2023](#); [Carniani et al. 2024](#); [Castellano et al. 2024](#); [Hsiao et al. 2023, 2024](#); [Zavala et al. 2025](#)), as well as the bright $z > 10$ CEERS galaxies from [Arrabal](#)

Haro et al. (2023a,b). Since the SFR_{10} values are not reported for the CEERS objects, we have re-fit them using BAGPIPES following our methodology outlined in Section 3.4. In cases where burstiness could not be robustly quantified, only upper limits are provided. We classify a galaxy as “bursting” if $\log_{10}(\text{SFR}_{10}/\text{SFR}_{100}) > 0$ (e.g., see Endsley et al. 2024a); our results are shown in Figure 4.

To statistically assess the significance of stochastic star formation among these 12 galaxies, we performed a Monte Carlo Markov Chain (MCMC) resampling of each derived $\log_{10}(\text{SFR}_{10}/\text{SFR}_{100})$ value within its uncertainty, repeating this process $\sim 10^8$ times. The resulting distribution is shown in the right panel of Figure 4. A simple Gaussian fit to this distribution shows that indeed the sample of these galaxies can be considered bursting with a mean of $\mu = 0.30 \pm 0.02$ dex, albeit with a considerable scatter $\sigma = 0.42 \pm 0.02$ dex.

Before discussing the implications of our measurement, let us contrast our findings against simulated predictions of burstiness in bright galaxies at high redshift. We will start with analytic predictions. The median and width of the burstiness distribution can be interpreted in terms of an analytic model, where fluctuations on $\log \text{SFR}(t)$ are normally distributed with a known power-spectrum distribution (PSD, Caplar & Tacchella 2019; Iyer et al. 2020). The $\log_{10}(\text{SFR}_{10}/\text{SFR}_{100})$ statistic corresponds to a weighted integral over the PSD, and thus can be used to constrain the amplitude and timescale of burstiness. Following the methods described in Sun et al. (2024), we focus on the bright end of the UVLF at $z > 10$ and derive a median $\log_{10}(\text{SFR}_{10}/\text{SFR}_{100}) \sim -0.005$ (in agreement with zero in this toy case) and a scatter of 0.8 for a PSD amplitude $\sigma = 4$ and timescale $\tau_{\text{decor}} = 5$ Myr, which should also give rise to a high UV variability, though these parameters are degenerate. We plot the median and 68% confidence intervals of this distribution in Figure 4. We complement this comparison by including the burstiness metric results from the hydrodynamical FLARES simulations (Lovell et al. 2021; Wilkins et al. 2023b,c), focusing on the bright end of the UVLF ($M_{\text{UV}} \lesssim -20$) at $z \sim 11$, where the majority of our samples lies. In contrast to the simplified PSD toy model, the FLARES simulations strongly suggest that bright galaxies at high redshift are indeed bursting, with a tight distribution characterized by $\log_{10}(\text{SFR}_{10}/\text{SFR}_{100}) \sim 0.2$ and $\sigma \sim 0.08$. Our observed median burstiness is broadly consistent with both simulation predictions within 1σ . However, the large scatter in our measurements—driven primarily by the limited number of spectroscopically confirmed galaxies in our sample—makes

it difficult to assess the true statistical significance of this agreement.

Nonetheless, our results suggest that, on average, bright galaxies at $z > 10$ are in a bursting phase, with SFR_{10} exceeding SFR_{100} by approximately a factor of two. Although the NIRSpec/MSA selection function is challenging to fully characterize, spectroscopically confirmed samples of bright galaxies are expected to be largely complete. Moreover, these galaxies are selected based on their bright M_{UV} , rather than emission line intensities, implying that the selection is not intrinsically biased toward bursting systems—or against them.

To evaluate whether stochastic star formation may contribute to the observed overabundance of UV-bright galaxies at these redshifts, it is useful to compare the prevalence of burstiness at $z > 10$ to that at lower redshifts. We begin with the work by Endsley et al. (2024a), who used a photometrically selected sample of $\text{H}\alpha$ emitters at $z \sim 6$ and found a very tight burstiness distribution of $\log_{10}(\text{SFR}_3/\text{SFR}_{50}) \sim 0.16 \pm 0.04$ for galaxies with $M_{\text{UV}} < -20$. In a complementary study, Cole et al. (2025) analyzed a smaller, spectroscopically confirmed sample of bursting galaxies at similar redshifts, finding a broader distribution centered at $\sim -0.21 \pm 0.46$, with the large scatter driven by low number statistics—similar to our case.

Both observational results at $z \sim 6$ are ~ 0.1 dex and ~ 0.5 dex lower, respectively, than the median burstiness derived in our work. This difference may hint that, at least among $M_{\text{UV}} < -20$ galaxies, burstiness is a more prominent feature at $z > 10$ than at later times, suggesting that stochastic star-formation could at least in-part drive the overabundance of UV-bright objects at early times. However, given the large scatter in our measured distribution, it remains difficult to determine with high confidence whether this trend is significant. To reach the level of precision afforded by both photometric samples and simulations, the number of confirmed high-redshift galaxies would need to increase by at least a factor of ~ 9 (i.e., $1/\sqrt{N}$), in order to reduce the scatter in our observed distribution by a factor of ~ 3 , to match lower uncertainties found in e.g. Endsley et al. (2024b). Continued spectroscopic follow-up of bright galaxies at $z > 10$ with *JWST* will be critical in establishing whether bursting star formation is indeed a defining feature of the earliest galaxies.

5. CONCLUSIONS

We present spectroscopic identification of two $z > 10$ galaxies obtained with the first 14% of the CAPERS MSA observations. Both objects present a clear $\text{Ly}\alpha$ break which results in unambiguous redshifts of $z =$

10.562 and $z = 11.013$. We examine physical properties of both galaxies via SED fitting and empirically as well as morphologies and star formation histories, finding evidence for recent bursting star formation in CAPERS_UDS_z10, thanks to the detection of strong ($EW_0 \sim 70 \text{ \AA}$) $H\gamma$ emission. The latter object CAPERS_UDS_z11, lacks any Balmer emission lines detected at high significance, preventing us from securely confirming or ruling out an ongoing burst, however it does present a tentatively detected O II emission line.

We combine our sample with all other bright $M_{UV} < -20$ galaxies at $z > 10$ from recent literature (Arrabal Haro et al. 2023a,b; Álvarez-Márquez et al. 2024; Bunker et al. 2023; Carniani et al. 2024; Castellano et al. 2024; Hsiao et al. 2023; Fujimoto et al. 2024; Napolitano et al. 2025) and explore what role stochastic star formation has had in shaping early galaxy formation. We find that the bright end of the UVLF at $z > 10$ is likely to be dominated by galaxies observed during an ongoing starburst, as characterized by a median $\log_{10}(\text{SFR}_{10}/\text{SFR}_{100}) \sim 0.30$ dex, with a scatter of $\sigma \sim 0.42$ dex.

Determining the “burstiness” of a galaxy typically requires a well-constrained SFH to reliably estimate the SFR within the last 10 Myr. However, this becomes particularly challenging at $z > 10$, as we have discussed, where typical strong emission lines such as $H\beta$ and [O III], redshift beyond NIRSpect spectral coverage, thus making such measurements increasingly uncertain. While one can still place upper limits on burstiness either through SED fitting or empirically via non-detections of emission lines, these approaches are inherently limited and subject to significant degeneracies—underscoring the need for deeper (and wider) spectroscopic data to robustly trace recent star formation activity at early cosmic times. In the next few months CAPERS is expected to double the number of galaxies at $z > 10$, thus yielding us the much needed statistical certainty to determine the true impact (or lack thereof) of bursting SF on the early galaxy physics.

ACKNOWLEDGMENTS

The authors would like to thank Richard Ellis for insightful discussions about bursting star-formation at high redshift, the PRIMER team for carrying out *JWST* imaging of the UDS, and notably Dan Magee for reducing the PRIMER NIRCcam data. VK acknowledges support from the University of Texas at Austin Cosmic Frontier Center. AT and SF acknowledge support from NASA through grant JWST-GO-6368. LN acknowledges support from grant “Progetti per Avvio alla Ricerca - Tipo 1, Unveiling Cosmic Dawn: Galaxy Evolution with CAPERS” (AR1241906F947685). PGP-G acknowledges support from grant PID2022-139567NB-I00 funded by Spanish Ministerio de Ciencia e Innovación MCIN/AEI/10.13039/501100011033, FEDER *Una manera de hacer Europa*. This work is based on observations made with the NASA/ESA/CSA *James Webb Space Telescope*, obtained at the Space Telescope Science Institute, which is operated by the Association of Universities for Research in Astronomy, Incorporated, under NASA contract NAS5-03127. Support for program number GO-6368 was provided through a grant from the STScI under NASA contract NAS5-03127. The data presented in this article were obtained from the Mikulski Archive for Space Telescopes (MAST) at the Space Telescope Science Institute. These observations are associated with program #6368.

Software: BAGPIPES (Carnall et al. 2019), BEAGLE (Chevallard & Charlot 2016), EAZY (Brammer et al. 2008), GALFIT (Peng et al. 2002), grizli (Brammer 2023), sep (Barbary 2016), SExtractor (Bertin & Arnouts 1996)

Facilities: *JWST*, *HST*

REFERENCES

- Álvarez-Márquez, J., Crespo Gómez, A., Colina, L., et al. 2024, arXiv e-prints, arXiv:2412.12826, doi: [10.48550/arXiv.2412.12826](https://doi.org/10.48550/arXiv.2412.12826)
- Arrabal Haro, P., Dickinson, M., Finkelstein, S. L., et al. 2023a, *Nature*, 622, 707, doi: [10.1038/s41586-023-06521-7](https://doi.org/10.1038/s41586-023-06521-7)
- . 2023b, *ApJL*, 951, L22, doi: [10.3847/2041-8213/acdd54](https://doi.org/10.3847/2041-8213/acdd54)
- Barbary, K. 2016, *Journal of Open Source Software*, 1, 58, doi: [10.21105/joss.00058](https://doi.org/10.21105/joss.00058)
- Behroozi, P. S., & Silk, J. 2015, *ApJ*, 799, 32, doi: [10.1088/0004-637X/799/1/32](https://doi.org/10.1088/0004-637X/799/1/32)
- Bertin, E., & Arnouts, S. 1996, *A&AS*, 117, 393, doi: [10.1051/aas:1996164](https://doi.org/10.1051/aas:1996164)
- Bouwens, R., Illingworth, G., Oesch, P., et al. 2023a, *MNRAS*, 523, 1009, doi: [10.1093/mnras/stad1014](https://doi.org/10.1093/mnras/stad1014)
- Bouwens, R. J., Illingworth, G. D., Oesch, P. A., et al. 2015, *ApJ*, 803, 34, doi: [10.1088/0004-637X/803/1/34](https://doi.org/10.1088/0004-637X/803/1/34)
- Bouwens, R. J., Oesch, P. A., Stefanon, M., et al. 2021, *AJ*, 162, 47, doi: [10.3847/1538-3881/abf83e](https://doi.org/10.3847/1538-3881/abf83e)
- Bouwens, R. J., Stefanon, M., Brammer, G., et al. 2023b, *MNRAS*, 523, 1036, doi: [10.1093/mnras/stad1145](https://doi.org/10.1093/mnras/stad1145)
- Boylan-Kolchin, M. 2023, *Nature Astronomy*, 7, 731, doi: [10.1038/s41550-023-01937-7](https://doi.org/10.1038/s41550-023-01937-7)
- Brammer, G. 2022, msaexp: NIRSpec analysis tools, 0.3, doi: [10.5281/zenodo.7299500](https://doi.org/10.5281/zenodo.7299500)
- Brammer, G. 2023, grizli, 1.8.2, Zenodo, Zenodo, doi: [10.5281/zenodo.7712834](https://doi.org/10.5281/zenodo.7712834)
- Brammer, G. B., van Dokkum, P. G., & Coppi, P. 2008, *ApJ*, 686, 1503, doi: [10.1086/591786](https://doi.org/10.1086/591786)
- Bromm, V., Coppi, P. S., & Larson, R. B. 2002, *ApJ*, 564, 23, doi: [10.1086/323947](https://doi.org/10.1086/323947)
- Bunker, A. J., Saxena, A., Cameron, A. J., et al. 2023, *A&A*, 677, A88, doi: [10.1051/0004-6361/202346159](https://doi.org/10.1051/0004-6361/202346159)
- Bushouse, H., Eisenhamer, J., Dencheva, N., et al. 2024, JWST Calibration Pipeline, 1.16.1, Zenodo, doi: [10.5281/zenodo.14153298](https://doi.org/10.5281/zenodo.14153298)
- Calzetti, D., Armus, L., Bohlin, R. C., et al. 2000, *ApJ*, 533, 682, doi: [10.1086/308692](https://doi.org/10.1086/308692)
- Caplar, N., & Tacchella, S. 2019, *MNRAS*, 487, 3845, doi: [10.1093/mnras/stz1449](https://doi.org/10.1093/mnras/stz1449)
- Carnall, A. C., McLure, R. J., Dunlop, J. S., & Davé, R. 2018, *MNRAS*, 480, 4379, doi: [10.1093/mnras/sty2169](https://doi.org/10.1093/mnras/sty2169)
- Carnall, A. C., McLure, R. J., Dunlop, J. S., et al. 2019, *MNRAS*, 490, 417, doi: [10.1093/mnras/stz2544](https://doi.org/10.1093/mnras/stz2544)
- Carnall, A. C., Begley, R., McLeod, D. J., et al. 2022, arXiv e-prints, arXiv:2207.08778, <https://arxiv.org/abs/2207.08778>
- Carniani, S., Hainline, K., D'Eugenio, F., et al. 2024, *Nature*, 633, 318, doi: [10.1038/s41586-024-07860-9](https://doi.org/10.1038/s41586-024-07860-9)
- Casey, C. M., Akins, H. B., Shuntov, M., et al. 2024, *ApJ*, 965, 98, doi: [10.3847/1538-4357/ad2075](https://doi.org/10.3847/1538-4357/ad2075)
- Castellano, M., Napolitano, L., Fontana, A., et al. 2024, *ApJ*, 972, 143, doi: [10.3847/1538-4357/ad5f88](https://doi.org/10.3847/1538-4357/ad5f88)
- Chabrier, G. 2003, *PASP*, 115, 763, doi: [10.1086/376392](https://doi.org/10.1086/376392)
- Chevallard, J., & Charlot, S. 2016, *MNRAS*, 462, 1415, doi: [10.1093/mnras/stw1756](https://doi.org/10.1093/mnras/stw1756)
- Chisholm, J., Berg, D. A., Endsley, R., et al. 2024, arXiv e-prints, arXiv:2402.18643, doi: [10.48550/arXiv.2402.18643](https://doi.org/10.48550/arXiv.2402.18643)
- Ciesla, L., Elbaz, D., Ilbert, O., et al. 2024, *A&A*, 686, A128, doi: [10.1051/0004-6361/202348091](https://doi.org/10.1051/0004-6361/202348091)
- Cleri, N. J., Olivier, G. M., Hutchison, T. A., et al. 2023, *ApJ*, 953, 10, doi: [10.3847/1538-4357/acde55](https://doi.org/10.3847/1538-4357/acde55)
- Cole, J. W., Papovich, C., Finkelstein, S. L., et al. 2025, *ApJ*, 979, 193, doi: [10.3847/1538-4357/ad9a6a](https://doi.org/10.3847/1538-4357/ad9a6a)
- Cullen, F., McLeod, D. J., McLure, R. J., et al. 2024, *MNRAS*, 531, 997, doi: [10.1093/mnras/stae1211](https://doi.org/10.1093/mnras/stae1211)
- Curtis-Lake, E., Carniani, S., Cameron, A., et al. 2023, *Nature Astronomy*, 7, 622, doi: [10.1038/s41550-023-01918-w](https://doi.org/10.1038/s41550-023-01918-w)
- Dayal, P., Ferrara, A., Dunlop, J. S., & Pacucci, F. 2014, *MNRAS*, 445, 2545, doi: [10.1093/mnras/stu1848](https://doi.org/10.1093/mnras/stu1848)
- Dekel, A., Sarkar, K. C., Birnboim, Y., Mandelker, N., & Li, Z. 2023, *MNRAS*, 523, 3201, doi: [10.1093/mnras/stad1557](https://doi.org/10.1093/mnras/stad1557)
- Donnan, C. T., Dunlop, J. S., McLure, R. J., McLeod, D. J., & Cullen, F. 2025, arXiv e-prints, arXiv:2501.03217, doi: [10.48550/arXiv.2501.03217](https://doi.org/10.48550/arXiv.2501.03217)
- Donnan, C. T., McLeod, D. J., Dunlop, J. S., et al. 2023, *MNRAS*, 518, 6011, doi: [10.1093/mnras/stac3472](https://doi.org/10.1093/mnras/stac3472)
- Donnan, C. T., McLure, R. J., Dunlop, J. S., et al. 2024, *MNRAS*, 533, 3222, doi: [10.1093/mnras/stae2037](https://doi.org/10.1093/mnras/stae2037)
- Ellis, R. S., McLure, R. J., Dunlop, J. S., et al. 2013, *ApJL*, 763, L7, doi: [10.1088/2041-8205/763/1/L7](https://doi.org/10.1088/2041-8205/763/1/L7)
- Endsley, R., Chisholm, J., Stark, D. P., Topping, M. W., & Whitler, L. 2024a, arXiv e-prints, arXiv:2410.01905, doi: [10.48550/arXiv.2410.01905](https://doi.org/10.48550/arXiv.2410.01905)
- Endsley, R., Stark, D. P., Whitler, L., et al. 2024b, *MNRAS*, 533, 1111, doi: [10.1093/mnras/stae1857](https://doi.org/10.1093/mnras/stae1857)
- Fakhouri, O., Ma, C.-P., & Boylan-Kolchin, M. 2010, *MNRAS*, 406, 2267, doi: [10.1111/j.1365-2966.2010.16859.x](https://doi.org/10.1111/j.1365-2966.2010.16859.x)
- Ferrara, A., Pallottini, A., & Dayal, P. 2023, *MNRAS*, 522, 3986, doi: [10.1093/mnras/stad1095](https://doi.org/10.1093/mnras/stad1095)
- Ferrara, A., Pallottini, A., & Sommovigo, L. 2025, *A&A*, 694, A286, doi: [10.1051/0004-6361/202452707](https://doi.org/10.1051/0004-6361/202452707)
- Finkelstein, S. L., Ryan, Russell E., J., Papovich, C., et al. 2015, *ApJ*, 810, 71, doi: [10.1088/0004-637X/810/1/71](https://doi.org/10.1088/0004-637X/810/1/71)

- Finkelstein, S. L., Bagley, M., Song, M., et al. 2022, *ApJ*, 928, 52, doi: [10.3847/1538-4357/ac3aed](https://doi.org/10.3847/1538-4357/ac3aed)
- Finkelstein, S. L., Leung, G. C. K., Bagley, M. B., et al. 2023, arXiv e-prints, arXiv:2311.04279, doi: [10.48550/arXiv.2311.04279](https://doi.org/10.48550/arXiv.2311.04279)
- . 2024, *ApJL*, 969, L2, doi: [10.3847/2041-8213/ad4495](https://doi.org/10.3847/2041-8213/ad4495)
- Finkelstein, S. L., Bagley, M. B., Arrabal Haro, P., et al. 2025, arXiv e-prints, arXiv:2501.04085, doi: [10.48550/arXiv.2501.04085](https://doi.org/10.48550/arXiv.2501.04085)
- Franco, M., Akins, H. B., Casey, C. M., et al. 2024, *ApJ*, 973, 23, doi: [10.3847/1538-4357/ad5e6a](https://doi.org/10.3847/1538-4357/ad5e6a)
- Fujimoto, S., Wang, B., Weaver, J. R., et al. 2024, *ApJ*, 977, 250, doi: [10.3847/1538-4357/ad9027](https://doi.org/10.3847/1538-4357/ad9027)
- Gelli, V., Mason, C., & Hayward, C. C. 2024, *ApJ*, 975, 192, doi: [10.3847/1538-4357/ad7b36](https://doi.org/10.3847/1538-4357/ad7b36)
- Grogin, N. A., Kocevski, D. D., Faber, S. M., et al. 2011, *ApJS*, 197, 35, doi: [10.1088/0067-0049/197/2/35](https://doi.org/10.1088/0067-0049/197/2/35)
- Harikane, Y., Ouchi, M., Oguri, M., et al. 2023, *ApJS*, 265, 5, doi: [10.3847/1538-4365/acaaa9](https://doi.org/10.3847/1538-4365/acaaa9)
- Harikane, Y., Inoue, A. K., Ellis, R. S., et al. 2024, arXiv e-prints, arXiv:2406.18352, doi: [10.48550/arXiv.2406.18352](https://doi.org/10.48550/arXiv.2406.18352)
- Hsiao, T. Y.-Y., Abdurro'uf, Coe, D., et al. 2023, arXiv e-prints, arXiv:2305.03042, doi: [10.48550/arXiv.2305.03042](https://doi.org/10.48550/arXiv.2305.03042)
- Hsiao, T. Y.-Y., Álvarez-Márquez, J., Coe, D., et al. 2024, *ApJ*, 973, 81, doi: [10.3847/1538-4357/ad6562](https://doi.org/10.3847/1538-4357/ad6562)
- Inayoshi, K., Harikane, Y., Inoue, A. K., Li, W., & Ho, L. C. 2022, *ApJL*, 938, L10, doi: [10.3847/2041-8213/ac9310](https://doi.org/10.3847/2041-8213/ac9310)
- Iyer, K. G., Tacchella, S., Genel, S., et al. 2020, *MNRAS*, 498, 430, doi: [10.1093/mnras/staa2150](https://doi.org/10.1093/mnras/staa2150)
- Katz, H., Saxena, A., Cameron, A. J., et al. 2023, *MNRAS*, 518, 592, doi: [10.1093/mnras/stac2657](https://doi.org/10.1093/mnras/stac2657)
- Kennicutt, Robert C., J. 1998, *ARA&A*, 36, 189, doi: [10.1146/annurev.astro.36.1.189](https://doi.org/10.1146/annurev.astro.36.1.189)
- Koekemoer, A. M., Faber, S. M., Ferguson, H. C., et al. 2011, *ApJS*, 197, 36, doi: [10.1088/0067-0049/197/2/36](https://doi.org/10.1088/0067-0049/197/2/36)
- Kokorev, V., Chisholm, J., Endsley, R., et al. 2024a, *ApJ*, 975, 178, doi: [10.3847/1538-4357/ad7d03](https://doi.org/10.3847/1538-4357/ad7d03)
- Kokorev, V., Atek, H., Chisholm, J., et al. 2024b, arXiv e-prints, arXiv:2411.13640, doi: [10.48550/arXiv.2411.13640](https://doi.org/10.48550/arXiv.2411.13640)
- Kravtsov, A., & Belokurov, V. 2024, arXiv e-prints, arXiv:2405.04578, doi: [10.48550/arXiv.2405.04578](https://doi.org/10.48550/arXiv.2405.04578)
- Larson, R. B. 1998, *MNRAS*, 301, 569, doi: [10.1046/j.1365-8711.1998.02045.x](https://doi.org/10.1046/j.1365-8711.1998.02045.x)
- Larson, R. L., Finkelstein, S. L., Kocevski, D. D., et al. 2023, arXiv e-prints, arXiv:2303.08918, doi: [10.48550/arXiv.2303.08918](https://doi.org/10.48550/arXiv.2303.08918)
- Leitherer, C., Ekström, S., Meynet, G., et al. 2014, *ApJS*, 212, 14, doi: [10.1088/0067-0049/212/1/14](https://doi.org/10.1088/0067-0049/212/1/14)
- Li, Z., Dekel, A., Sarkar, K. C., et al. 2024, *A&A*, 690, A108, doi: [10.1051/0004-6361/202348727](https://doi.org/10.1051/0004-6361/202348727)
- Looser, T. J., D'Eugenio, F., Maiolino, R., et al. 2023, arXiv e-prints, arXiv:2306.02470, doi: [10.48550/arXiv.2306.02470](https://doi.org/10.48550/arXiv.2306.02470)
- . 2024, *Nature*, 629, 53, doi: [10.1038/s41586-024-07227-0](https://doi.org/10.1038/s41586-024-07227-0)
- Lovell, C. C., Vijayan, A. P., Thomas, P. A., et al. 2021, *MNRAS*, 500, 2127, doi: [10.1093/mnras/staa3360](https://doi.org/10.1093/mnras/staa3360)
- Maiolino, R., Scholtz, J., Witstok, J., et al. 2023, arXiv e-prints, arXiv:2305.12492, doi: [10.48550/arXiv.2305.12492](https://doi.org/10.48550/arXiv.2305.12492)
- Mason, C. A., Trenti, M., & Treu, T. 2015, *ApJ*, 813, 21, doi: [10.1088/0004-637X/813/1/21](https://doi.org/10.1088/0004-637X/813/1/21)
- McLeod, D. J., McLure, R. J., & Dunlop, J. S. 2016, *MNRAS*, 459, 3812, doi: [10.1093/mnras/stw904](https://doi.org/10.1093/mnras/stw904)
- McLeod, D. J., Donnan, C. T., McLure, R. J., et al. 2024, *MNRAS*, 527, 5004, doi: [10.1093/mnras/stad3471](https://doi.org/10.1093/mnras/stad3471)
- McLure, R. J., Dunlop, J. S., Bowler, R. A. A., et al. 2013, *MNRAS*, 432, 2696, doi: [10.1093/mnras/stt627](https://doi.org/10.1093/mnras/stt627)
- Mitsubishi, I., Zavala, J. A., Bakx, T. J. L. C., et al. 2025, arXiv e-prints, arXiv:2501.19384, doi: [10.48550/arXiv.2501.19384](https://doi.org/10.48550/arXiv.2501.19384)
- Muñoz, J. B., Mirocha, J., Furlanetto, S., & Sabti, N. 2023, *MNRAS*, 526, L47, doi: [10.1093/mnrasl/sladi115](https://doi.org/10.1093/mnrasl/sladi115)
- Napolitano, L., Castellano, M., Pentericci, L., et al. 2024, arXiv e-prints, arXiv:2410.18763, doi: [10.48550/arXiv.2410.18763](https://doi.org/10.48550/arXiv.2410.18763)
- . 2025, *A&A*, 693, A50, doi: [10.1051/0004-6361/202452090](https://doi.org/10.1051/0004-6361/202452090)
- Oesch, P. A., Bouwens, R. J., Illingworth, G. D., Labbé, I., & Stefanon, M. 2018, *ApJ*, 855, 105, doi: [10.3847/1538-4357/aab03f](https://doi.org/10.3847/1538-4357/aab03f)
- Oesch, P. A., Brammer, G., van Dokkum, P. G., et al. 2016, *ApJ*, 819, 129, doi: [10.3847/0004-637X/819/2/129](https://doi.org/10.3847/0004-637X/819/2/129)
- Oke, J. B. 1974, *ApJS*, 27, 21, doi: [10.1086/190287](https://doi.org/10.1086/190287)
- Olivier, G. M., Berg, D. A., Chisholm, J., et al. 2022, *ApJ*, 938, 16, doi: [10.3847/1538-4357/ac8f2c](https://doi.org/10.3847/1538-4357/ac8f2c)
- Ono, Y., Harikane, Y., Ouchi, M., et al. 2023, *ApJ*, 951, 72, doi: [10.3847/1538-4357/acd44a](https://doi.org/10.3847/1538-4357/acd44a)
- Osterbrock, D. E. 1989, *Astrophysics of gaseous nebulae and active galactic nuclei*
- Papovich, C., Cole, J. W., Yang, G., et al. 2023, *ApJL*, 949, L18, doi: [10.3847/2041-8213/acc948](https://doi.org/10.3847/2041-8213/acc948)
- Peng, C. Y., Ho, L. C., Impey, C. D., & Rix, H.-W. 2002, *AJ*, 124, 266, doi: [10.1086/340952](https://doi.org/10.1086/340952)
- . 2010, *AJ*, 139, 2097, doi: [10.1088/0004-6256/139/6/2097](https://doi.org/10.1088/0004-6256/139/6/2097)
- Pérez-González, P. G., Costantin, L., Langeroodi, D., et al. 2023, *ApJL*, 951, L1, doi: [10.3847/2041-8213/acd9d0](https://doi.org/10.3847/2041-8213/acd9d0)

- Rix, H.-W., Barden, M., Beckwith, S. V. W., et al. 2004, *ApJS*, 152, 163, doi: [10.1086/420885](https://doi.org/10.1086/420885)
- Rodriguez-Gomez, V., Genel, S., Vogelsberger, M., et al. 2015, *MNRAS*, 449, 49, doi: [10.1093/mnras/stv264](https://doi.org/10.1093/mnras/stv264)
- Sérsic, J. L. 1963, *Boletín de la Asociacion Argentina de Astronomia La Plata Argentina*, 6, 41
- Shen, X., Vogelsberger, M., Boylan-Kolchin, M., Tacchella, S., & Kannan, R. 2023, *MNRAS*, 525, 3254, doi: [10.1093/mnras/stad2508](https://doi.org/10.1093/mnras/stad2508)
- Steinhardt, C. L., Kokorev, V., Rusakov, V., Garcia, E., & Sneppen, A. 2023, *ApJL*, 951, L40, doi: [10.3847/2041-8213/acdef6](https://doi.org/10.3847/2041-8213/acdef6)
- Sun, G., Faucher-Giguère, C.-A., Hayward, C. C., & Shen, X. 2023, *MNRAS*, 526, 2665, doi: [10.1093/mnras/stad2902](https://doi.org/10.1093/mnras/stad2902)
- Sun, G., Muñoz, J. B., Mirocha, J., & Faucher-Giguère, C.-A. 2024, arXiv e-prints, arXiv:2410.21409, doi: [10.48550/arXiv.2410.21409](https://doi.org/10.48550/arXiv.2410.21409)
- Tacchella, S., Finkelstein, S. L., Bagley, M., et al. 2022, *ApJ*, 927, 170, doi: [10.3847/1538-4357/ac4cad](https://doi.org/10.3847/1538-4357/ac4cad)
- Trussler, J. A. A., Conselice, C. J., Adams, N. J., et al. 2023, *MNRAS*, 525, 5328, doi: [10.1093/mnras/stad2553](https://doi.org/10.1093/mnras/stad2553)
- Tumlinson, J. 2006, *ApJ*, 641, 1, doi: [10.1086/500383](https://doi.org/10.1086/500383)
- Weibel, A., de Graaff, A., Setton, D. J., et al. 2024, arXiv e-prints, arXiv:2409.03829, doi: [10.48550/arXiv.2409.03829](https://doi.org/10.48550/arXiv.2409.03829)
- Wilkins, S. M., Lovell, C. C., Irodotou, D., et al. 2023a, arXiv e-prints, arXiv:2305.18175, doi: [10.48550/arXiv.2305.18175](https://doi.org/10.48550/arXiv.2305.18175)
- Wilkins, S. M., Vijayan, A. P., Lovell, C. C., et al. 2023b, *MNRAS*, 519, 3118, doi: [10.1093/mnras/stac3280](https://doi.org/10.1093/mnras/stac3280)
- . 2023c, *MNRAS*, 518, 3935, doi: [10.1093/mnras/stac3281](https://doi.org/10.1093/mnras/stac3281)
- Witstok, J., Jakobsen, P., Maiolino, R., et al. 2024, arXiv e-prints, arXiv:2408.16608, doi: [10.48550/arXiv.2408.16608](https://doi.org/10.48550/arXiv.2408.16608)
- Yang, L., Morishita, T., Leethochawalit, N., et al. 2022, *ApJL*, 938, L17, doi: [10.3847/2041-8213/ac8803](https://doi.org/10.3847/2041-8213/ac8803)
- Yung, L. Y. A., Somerville, R. S., Finkelstein, S. L., Popping, G., & Davé, R. 2019, *MNRAS*, 483, 2983, doi: [10.1093/mnras/sty3241](https://doi.org/10.1093/mnras/sty3241)
- Yung, L. Y. A., Somerville, R. S., Finkelstein, S. L., et al. 2020, *MNRAS*, 496, 4574, doi: [10.1093/mnras/staa1800](https://doi.org/10.1093/mnras/staa1800)
- Yung, L. Y. A., Somerville, R. S., Finkelstein, S. L., Wilkins, S. M., & Gardner, J. P. 2024, *MNRAS*, 527, 5929, doi: [10.1093/mnras/stad3484](https://doi.org/10.1093/mnras/stad3484)
- Zavala, J. A., Castellano, M., Akins, H. B., et al. 2025, *Nature Astronomy*, 9, 155, doi: [10.1038/s41550-024-02397-3](https://doi.org/10.1038/s41550-024-02397-3)